UKPMC Funders Group Author Manuscript

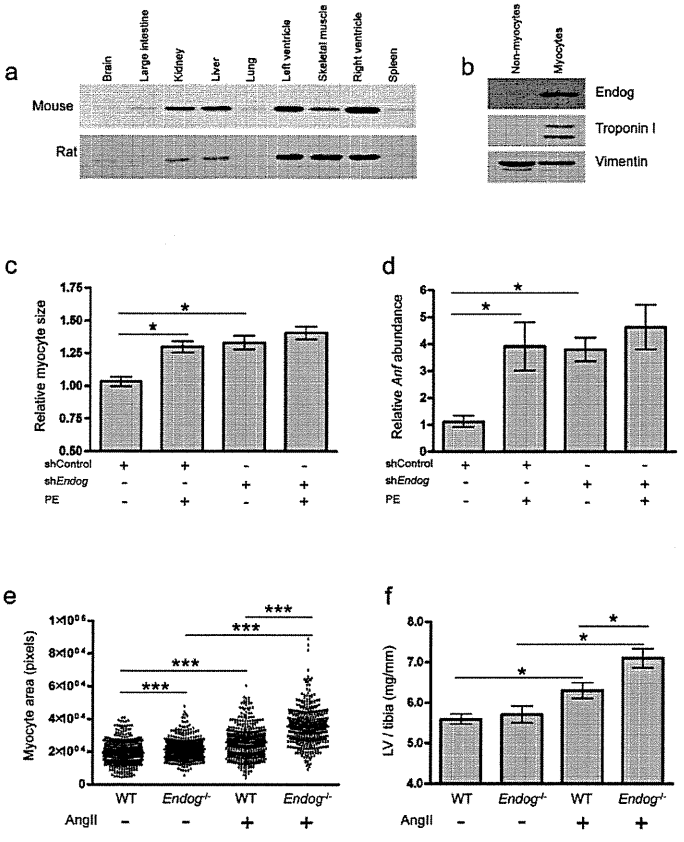

Figure 2. *Endog* regulates cardiac hypertrophy

a, Immunoblot of Endog expression in mouse and rat tissues (Endog: ~30 kDa). **b**, Immunoblot of Endog expression in myocyte and non-myocyte populations isolated from neonatal rat heart. **c**, Cardiomyocyte size (n≥100 cells, n=3 independent experiments) treated with shRNA against *Endog* (sh*Endog*) or control shRNA (shControl) in the presence or absence of the hypertrophic stimulant phenylephrine (PE, 100μM, 24 h). **d**, Expression of the hypertrophic biomarker *Anf* in sh*Endog* and shControl treated cells. **e**, Cardiomyocyte size (Supplementary Fig. 5) in *Endog*$^{-/-}$ and wildtype (WT) mice at baseline and following angiotensin II-induced cardiac hypertrophy. **f**, LVM/tibial length in *Endog*$^{-/-}$ and WT mice at baseline and following AngII stimulation. Data are represented as mean+s.e.m. *, $P<0.05$, **, $P<0.01$, ***, $P<0.001$.

UKPMC Funders Group Author Manuscript

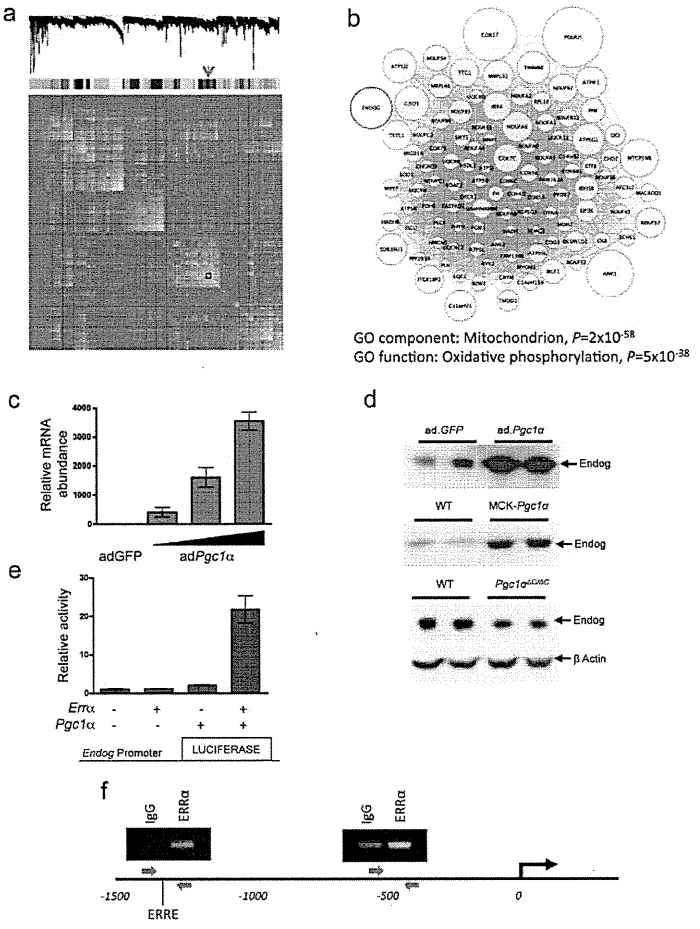

Figure 3. *ENDOG* is co-expressed with a mitochondrial-specific gene network and regulated by *Pgc1α* and *ERRα*

a, Genes (8,490 from 210 datasets) are clustered and plotted based on the dissimilarity metric between their expression profiles (Supplementary Methods). From top to bottom: low-hanging branches in the dendrogram represent groups of genes (modules) that have a high similarity metric. Modules are shown beneath the dendrogram and are colour coded. The arrow indicates the module (also boxed) containing *ENDOG*. In the heat-map of the correlations between expression profiles, high and low similarities are coloured yellow and red, respectively. **b**, Weighted gene co-expression network analysis (WGCNA[23]) for the module containing *ENDOG*, providing functional annotation by cellular localization by Gene Ontology classification (Supplementary Tables 2 and 3). Nodes represent genes and edges represent significant co-expression between genes. The node size is proportional to the relative degree of interconnectivity of each gene within the module. **c**, QPCR analysis of *Endog* expression in cultured cardiomyocytes following infection with adenovirus (ad) expressing *GFP* (ad.*GFP*) or *Pgc1α* (ad.*Pgc1α*). **d**, Immunoblot of Endog expression in ad.*Pgc1α*-infected cardiomyocytes (top panel), skeletal muscle of wild-type (WT) mice and transgenic mice expressing *Pgc1α* under the control of muscle creatine kinase (MCK-*Pgc1α*) (middle panel), and in hearts of WT and cardiac-specific *Pgc1α* deleted mice ($Pgc1\alpha^{\Delta C/\Delta C}$) (bottom panel). **e**, *Endog* promoter activity in HEK293 cells infected with ad.*Pgc1α* and and/or ad.*Errα*. **f**, ERRα chromatin immunoprecipitation (ChIP) and PCR of two regions of the *ENDOG* promoter. Red arrows denote primers and ERRE specifies the

location of a consensus ERR response element (1304 bases upstream). The experiment was repeated three times with similar results and PCR products quantified by QPCR.

UKPMC Funders Group Author Manuscript

UKPMC Funders Group Author Manuscript

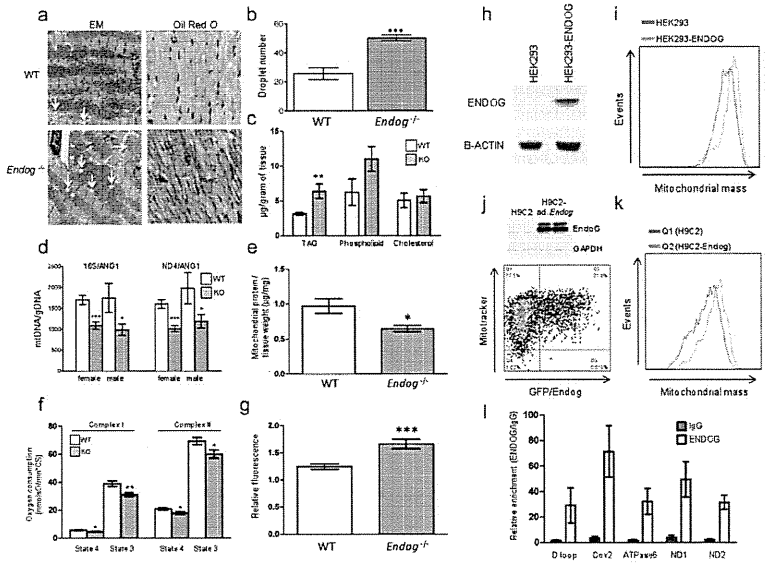

Figure 4. *Endog* regulates mitochondrial function and cardiac lipid metabolism

a, Transmission electron micrographs and oil red *O* stained micrographs (high resolution, Supplementary Fig. 7) of left ventricular sections from WT and *Endog*$^{-/-}$ mice. **b,** Quantification of the number of mitochondrial-associated droplets in WT and *Endog*$^{-/-}$ mice. **c**, Quantification of cardiac triglyceride (TAG), phospholipid and cholesterol content in WT and *Endog*$^{-/-}$ mice (n=5). **d**, Ratio of mitochondrial DNA (mtDNA) to genomic DNA (gDNA) in hearts of WT and *Endog*$^{-/-}$ mice. **e,** Quantification of mitochondrial protein content in WT and *Endog*$^{-/-}$ mice (n=5). **f**, State 3 and state 4 oxygen consumption in the presence of complex I or complex II substrates in isolated cardiac mitochondria from WT (n=6) and *Endog*$^{-/-}$ (n=5) mice. **g**, Relative fluorescence-based measurement of ROS production by mitochondria isolated from WT (n=6) and *Endog*$^{-/-}$ (n=5) mice. **h-k**, Representative flow cytometry analysis of mitochondrial mass in HEK293 and H9C2 cells over-expressing ENDOG or Endog, respectively (n=4). **h**, Stable expression of *ENDOG* in HEK293 cells (HEK293-*ENDOG*). **i,** Flow cytometry analysis of HEK293 and HEK293-*ENDOG* cells stained with mitotracker. **j,** Adenovirus (ad)-mediated expression of GFP and Endog in myocytes and flow cytometry analysis of ad.*Endog* infected cells (Q2) and uninfected control cells (Q1). **k**, Number of events plotted against mitochondrial mass in ad.*Endog* infected (Q2) and control (Q1) H9C2 cells. **l**, QPCR of mtDNA-protein complexes following ChIP of mitochondrial chromatin using anti-ENDOG antibody or IgG. All data are represented as mean+s.e.m. *, $P<0.05$, **, $P<0.01$, ***, $P<0.001$.

Kuramoto *et al. BMC Genetics* 2011, **12**:91
http://www.biomedcentral.com/1471-2156/12/91

BMC Genetics

RESEARCH ARTICLE Open Access

A rat model of hypohidrotic ectodermal dysplasia carries a missense mutation in the *Edaradd* gene

Takashi Kuramoto*, Mayuko Yokoe, Ryoko Hashimoto, Hiroshi Hiai and Tadao Serikawa

Abstract

Background: Hypohidrotic ectodermal dysplasia (HED) is a congenital disorder characterized by sparse hair, oligodontia, and inability to sweat. It is caused by mutations in any of three Eda pathway genes: ectodysplasin (*Eda*), Eda receptor (*Edar*), and Edar-associated death domain (*Edaradd*), which encode ligand, receptor, and intracellular adaptor molecule, respectively. The Eda signaling pathway activates NF-κB, which is central to ectodermal differentiation. Although the causative genes and the molecular pathway affecting HED have been identified, no curative treatment for HED has been established. Previously, we found a rat spontaneous mutation that caused defects in hair follicles and named it sparse-and-wavy (*swh*). Here, we have established the *swh* rat as the first rat model of HED and successfully identified the *swh* mutation.

Results: The *swh/swh* rat showed sparse hair, abnormal morphology of teeth, and absence of sweat glands. The ectoderm-derived glands, meibomian, preputial, and tongue glands, were absent. We mapped the *swh* mutation to the most telomeric part of rat Chr 7 and found a Pro153Ser missense mutation in the *Edaradd* gene. This mutation was located in the death domain of EDARADD, which is crucial for signal transduction and resulted in failure to activate NF-κB.

Conclusions: These findings suggest that *swh* is a loss-of-function mutation in the rat *Edaradd* and indicate that the *swh/swh* rat would be an excellent animal model of HED that could be used to investigate the pathological basis of the disease and the development of new therapies.

Background

Hypohidrotic ectodermal dysplasia (HED) is a genetic disorder characterized by sparse hair, oligodontia, reduced sweating, and defects in a number of other ectodermal organs [1]. A lack of sweat glands can lead to recurrent severe overheating. Thus, children with HED are at substantial risk of sudden death in infancy due to fatal hyperpyrexia [2].

HED is caused by mutations in any of the three Eda pathway genes: ectodysplasin (*Eda*) [3,4], ED receptor (*Edar*) [5], and EDAR-associated death domain (*Edaradd*) [6]. They encode the ligand, receptor, and intracellular signal mediator of a single linear pathway, respectively. The Eda signaling pathway activates transcription factor NF-κB thereby playing an important role in embryonic development, especially in the development of ectodermally derived organs [1].

In humans, there are three types of HED with different inheritance: X-linked HED, autosomal dominant HED, and autosomal recessive HED. X-linked HED is the most common form of HED and is caused by mutations in *EDA*. Autosomal HED is caused by mutations in *EDAR* or *EDARADD*. Currently, over 100 different mutations in the *EDA* gene are known, while only ~20 and 4 causative mutations have been found in *EDAR* and *EDARADD*, respectively [7].

To date, four mouse models of HED are available: *Tabby, downless, Sleek*, and *crinkled*. The mutant phenotype of the *Tabby* mouse is inherited in an X-linked manner and the *Tabby* mouse carries a mutation in the *Eda* gene [4]. The recessive *downless* and dominant *Sleek* mice carry mutations in the *Edar* gene [8]. The *crinkled* mouse carries a mutation in the *Edaradd* gene [6]. The phenotypes in *Eda, Edar*, and *Edaradd* mutant mice are almost identical and include abnormalities in teeth, hair, and sweat glands, the triad of symptoms of HED. Over 20 different glands, including lacrimal, meibomian, salivary,

* Correspondence: tkuramot@anim.med.kyoto-u.ac.jp
Institute of Laboratory Animals, Graduate School of Medicine, Kyoto University, Yoshidakonoe-cho, Sakyo-ku, Kyoto 606-8501, Japan

submandibular, and mammary glands, are also affected [9-11]. These mutant mice have been used to study the roles of the Eda pathway in the development and morphogenesis of ectoderm-derived organs and to develop a novel treatment for HED using a recombinant EDA protein [12].

Mutations in some of the genes in the Eda pathway have been identified in various species, such as medaka [13], zebrafish [14], cattle [15-18], and dog [19]. Analyses of these mutations showed critical roles of the Eda pathway in the development of epithelial appendages, as well as in morphological evolution. Thus, the identification of novel mutations in different species emphasized the importance of the Eda pathway, and enabled the phenotypes of the mutated animals to be compared, giving new insights into the functions of the Eda pathway. If such novel mutations can be identified in mammals, then the affected species could be used as a disease model of HED.

In a previous study, we described a mutant rat, sparse and wavy hair (*swh*), which arose spontaneously in a colony of inbred WTC rats in 1998 [20]. The mutant phenotype is characterized by sparse and wavy hair, impaired body weight gain, and hypoplasticity of the mammary gland. The hair follicles in these rats were reduced both in number and size, a characteristic associated with hypoplasia of both the sebaceous glands and the subcutaneous fat tissues. The mammary glands of *swh/swh* female rats were hypoplastic and differentiation of mammary epithelial and myoepithelial cells was impaired. Thus, it is conceivable that the *swh/swh* rat will provide a good experimental model to clarify the mechanisms involved in the development of skin appendages, most of which are derived from ectoderm [20].

In our previously reported linkage analysis, *swh* mapped to the telomeric part of rat Chr 17. At that time, the physical location of the *swh* locus could not be accurately determined because a SSLP marker, *D17Rat140*, which defined the distal side of the *swh* locus was, in the earlier public rat genome linkage map, erroneously assigned to the middle part of Chr 17 and not to the telomeric part of Chr 17. Recently, with the development of more than 20,000 single nucleotide polymorphism (SNP) markers for 167 rat inbred strains and with the haplotype mapping data from the genotyping of these SNPs, the genome linkage map has been improved [21]. In the improved rat genome map, *D17Rat140* and its neighboring genes are correctly mapped to the telomeric part of rat Chr 17. Thus, in addition to the 24 candidate genes selected from our previous linkage analysis, we also considered these newly mapped genes to be candidates of *swh* [20].

In this study, to demonstrate the suitability of the *swh* rat as an HED model, we investigated the pathology of tissues and organs in which morphological abnormalities in HED are known to occur. Furthermore, we identified the causative mutation of the *swh* phenotype using a positional cloning approach, and found a missense mutation in the death domain of EDARADD, that might explain the inability of the mutant *Edaradd* gene to activate NF-κB. Our findings suggest that *swh* is a loss-of-function mutation of the rat *Edaradd* and support the *swh/swh* rat as an excellent animal model of HED that can be used to investigate the pathological basis of the disease and to develop new therapies.

Methods

Animals

ACI/NKyo, WTC/Kyo, and WTC-*swh*/Kyo rats were provided by the Japanese National BioResource Project for the Rat and kept in our animal facility for all experiments in this study. Animal care and experimental procedures were approved by the Animal Research Committee, Kyoto University, Japan, and were conducted according to the Regulation on Animal Experimentation at Kyoto University.

Histopathology

For light microscopy, the tongue, eyelid, ventral skin, footpad, and preputial gland were harvested from WTC-*swh/swh* and WTC rats at 8 weeks of age. Tissues were fixed in 10% neutral-buffered formalin, embedded in paraffin, and stained with hematoxylin and eosin (HE).

Sweat tests and whole mount staining of mammary glands

The sweat test was performed as described previously [12]. Briefly, the hind paws of rats anesthetized with sevoflurane were painted with a solution of 3% (wt/vol) iodine in ethanol. Once dry, the paws were painted with a suspension of 40% (wt/vol) starch I mineral oil. Photographs were taken 1 min later and sweat was detected as dark spots. Mammary glands were prepared as a whole mount and stained as described previously [22].

Fine mapping of swh

For fine mapping of *swh*, F2 animals (n = 769) were produced by intercrossing (ACI/NKyo × WTC-*swh*) F1 rats. Homozygous *swh/swh* animals were identified at 3-4 weeks of age based on the appearance of the sparse-and-waved hair phenotype. One hundred and ninety-eight *swh/swh* homozygotes were used for fine mapping of *swh*. Genomic DNA was prepared from tail biopsies using the automatic DNA purification system (PI-200; Kurabo, Japan).

RNA extraction, RT-PCR and direct sequencing

Total RNA was extracted from the skin of 2-week-old animals. RNA preparation, RT-PCR and direct sequencing of PCR products were performed as described

previously [23]. Rat *Edaradd* cDNAs were amplified with 6 sets of primers (Table 1). The PCR products overlapped each other and spanned the entire coding sequence of *Edaradd*.

Transient transfection and reporter assays

The NF-κB assay was designed to test for activation of the NF-κB responsive promoter. HEK293T cells grown in poly-L-lysine coated 24-well plates were transfected using SuperFect (Qiagen) with 1.2 μg pNF-κB-Luc (Clontech), 2 μg pRL-TK, and an increasing amount of expression vectors encoding the wild-type EDARADD or the *swh*-type EDARADD (Pro153Ser). The Luc reporter of the pNF-κB-Luc encodes firefly luciferase. The HSV-TK (herpes simplex virus thymidine kinase) promoter drives renilla luciferase in pRL-TK. Total DNA was adjusted to 2.6 μg by adding pCMV-HA (Clontech) vector as necessary. Luciferase activity was measured using the Dual-Luciferase Reporter Assay System (Promega) 48 h after transfection, according to the manufacturer's protocol.

Results

Phenotypes of *swh/swh* rat as hypohidrotic ectodermal dysplasia (HED)

Patients with HED display defective development of hair, teeth, sweat glands, and several exocrine glands, such as sebaceous, salivary, meibomian, and lacrimal [1,24]. To evaluate the relevance of the *swh/swh* rat as a HED model, we looked for developmental defects in those tissues of *swh/swh* rats. In addition to defects of the hair, skin, and mammary glands, which have been reported previously [20] (Figure 1A, B), we found defects in the sweat, meibomian, preputial, and tongue glands. In these tissues, the exocrine glands were absent in the *swh/swh* rats (Figure 1C, D, E, F). In the sweat test, no sweat was detected in *swh/swh* rats, indicating that the sweat glands were functionally defective (Figure 1C). We also found a reduced number of cusps in the lower first molars in the *swh/swh* rats (Figure 1G).

In the Eda pathway mutant mice, *Tabby, downless,* and *crinkled,* a kinked tail tip, a bald patch behind the ear, and abnormal pelage hair composition are characteristic. Similarly, in *swh/swh* rat, the pelage hair was composed of only an abnormal awl hair (Figure 1A); however, the tail had hair on it, the frequency of kinked tail was low, and the bald patch behind the ear was not found (Figure 1G).

These findings indicate that the mutant phenotypes of *swh/swh* rats are similar to developmental defects in HED patients and in the established mouse models; therefore, it is likely that the *swh/swh* rat will be suitable as a model of HED.

Positional cloning of *swh*

In a previous study, we mapped *swh* to rat Chr 17 [20]. To more specifically map the position of the *swh* locus, we genotyped F2 intercross progeny for markers known to be closely linked to *swh*. There was only one recombinant chromosome between *swh* and either *D17Rat132* or *D17Rat140* in 396 meioses (= 198 × 2) and we were able to map *swh* to the most distal part of Chr17 (Figure 2A). The rat genome map (RGSC v3.4) showed two genes in the *swh* locus, *Ero1lb* (ERO1-like beta (*S. cerevisiae*)) and *Edaradd* (ectodysplasin-A receptor-associated death domain). The mouse mutant of *Edaradd* is called *crinkled* (*cr*) and mice that carry this mutation show a sparse hair phenotype that is similar to that of the *swh* rat [25]. Additionally, mutations in the human *EDARADD* gene have been found in families affected with HED [6,26]. Thus, we considered *Edaradd* as a good candidate of *swh*. Although the abnormal expression of *Edaradd* mRNA was not detected in the skin of *swh/swh* rats (data not shown), we found a missense mutation (C to T) in exon 6 of the *swh/swh Edaradd* gene. This mutation was deduced to change proline to serine at the 153rd amino acid (Pro153Ser) of the rat EDARADD protein (Figure 2B). The 153rd amino acid is located in the death domain of EDARADD and is highly conserved in vertebrates (Figure 2C). These findings suggest that the Pro153Ser missense mutation of the *Edaradd* gene is causative of the phenotypes of *swh/swh* rats.

Reporter assay for the Pro153Ser mutant EDARADD

Overexpression of *Edaradd* in 293T cells activates NF-κB in a dose-dependent manner [25]. To examine whether Pro153Ser *Edaradd* can activate NF-κB, we carried out a reporter assay. As shown in Figure 3, wild-type *Edaradd*

Table 1 PCR primers used to amplify rat *Edaradd* cDNA

Primer set	Forward (5' > 3')	Reverse (5' > 3')
Edaradd-1&2	CTGAGAGAGAGTCGCGCATT	GCCACAGCTGTTCCCATAG
Edaradd-3&4	GCCCAGAAAAGGCAGCTC	GGAAAACCTTTGGAGTTTCTGA
Edaradd-5&6	CGATGAGCCAGCTTTACCTC	GGATAATTGGGTAACTATTCTCAACC
Edaradd-7&8	TCCATCCCAATTTTACCAACA	CGGCAAGCATTTTAATGACC
Edaradd-9&10	CAGTCAGCCCCTTGCACT	GCATGCTCTCATCAACATGG
Edaradd-11&12	TGTCACCAATGTGGTAGAAAAA	CAGGGATAACCACTGCCTGT

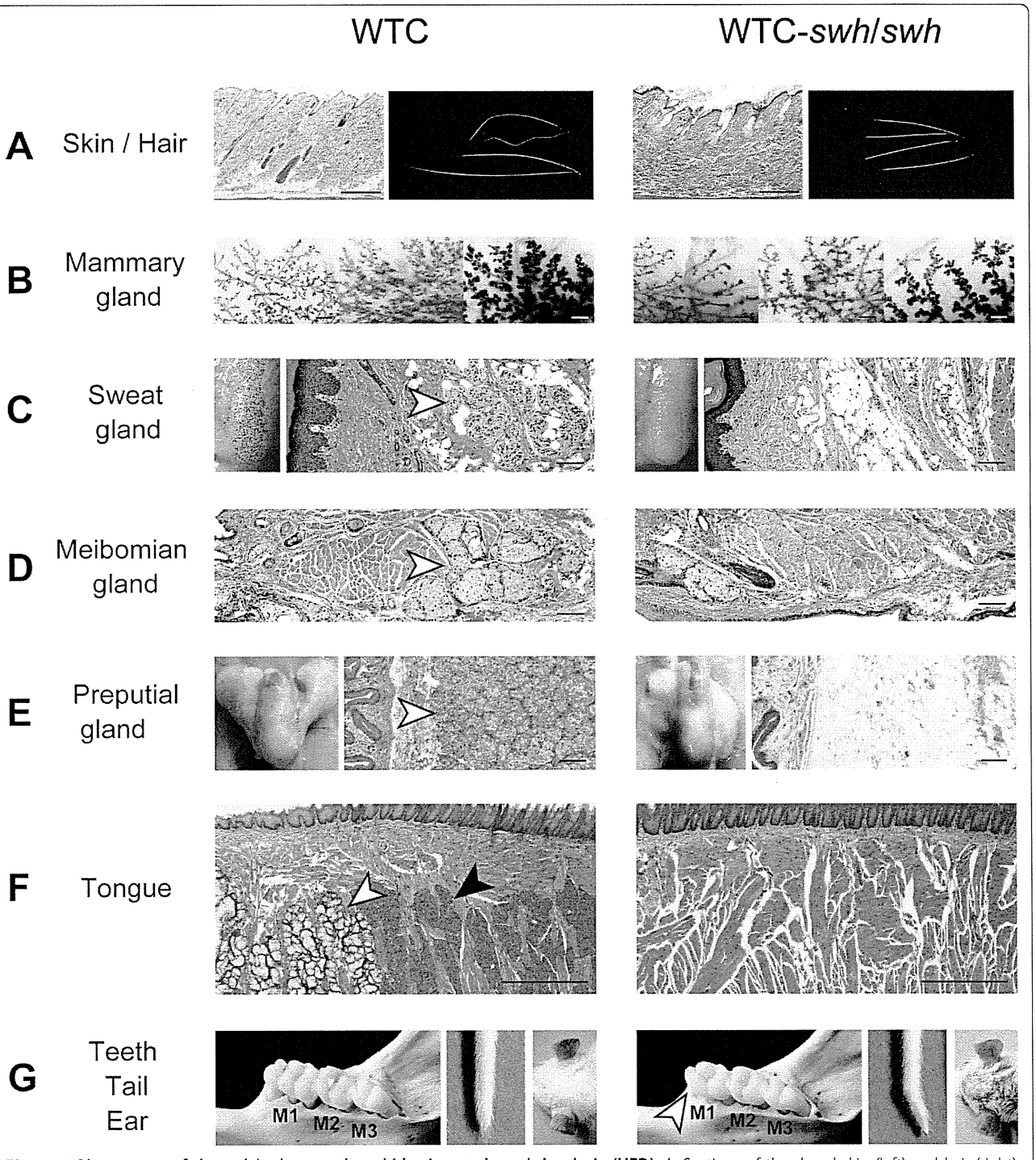

Figure 1 Phenotypes of the swh/swh rat as hypohidrotic ectodermal dysplasia (HED). A, Sections of the dorsal skin (left) and hair (right). Incomplete hair follicles are evident in *swh/swh* rat. Scale bar, 0.5 mm. The WTC rat has four hair types; auchene, zigzag, awl and guard, while the *swh/swh* rat have only the abnormal awl hair. B, Whole mount stained mammary glands; 6-week-old (left), 8-week-old (center), and pregnant day 9 (right). Mammary gland branching is poor in *swh/swh* rat. Scale bar, 1 mm. C, Sweat test results (left) and section of the footpads. Sweat, detected as dark spots, is not seen in *swh/swh* rat. Sweat glands (arrowhead) are present in WTC rat and absent in *swh/swh* rat. Scale bar, 100 μm. D, Sections of the eyelid. The meibomian glands (arrowhead) are present in WTC rat and absent in *swh/swh* rat. Scale bar, 100 μm. E, An entire view (left) and a section of the preputial gland (right). The preputial gland is atrophied in male *swh/swh* rat. Acinous glands (arrowhead) are present in WTC rat and absent in *swh/swh* rat. Scale bar, 100 μm. F, Section of the tongue. Both mucous (open arrowhead) and serous (filled arrowhead) glands are present in WTC rat and neither is seen in *swh/swh* rat. Scale bar, 0.5 mm. **G**, Buccal views of lower molars (left), tip of tail (center), and posterior auricular region (right). Cusp number is reduced in the first molar (arrow head) in *swh/swh* rat. Some *swh/swh* rats show the kink tail. The bald patch behind the ear was not evident in the *swh/swh* rat.

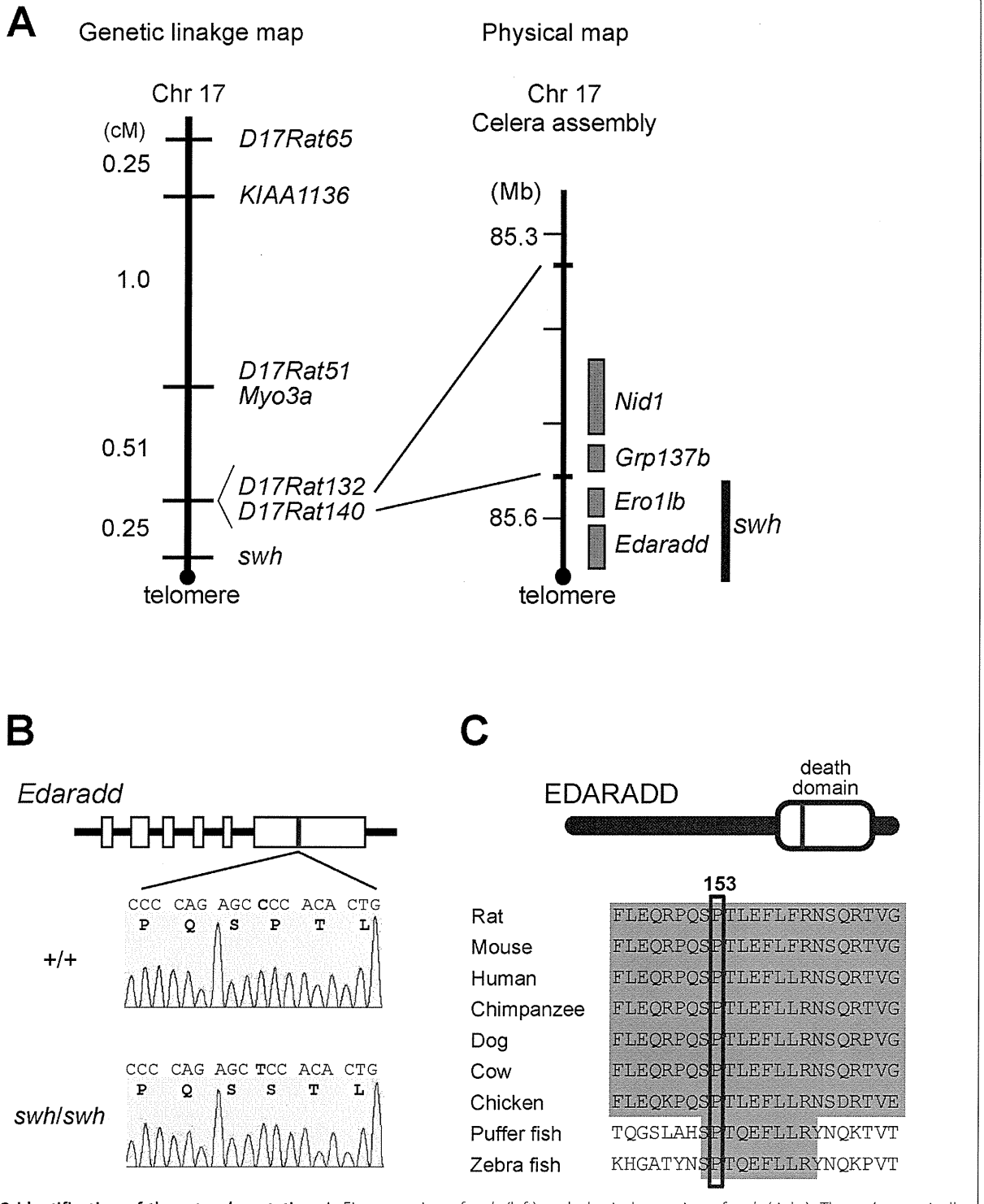

Figure 2 Identification of the rat *swh* mutation. A, Fine mapping of *swh* (left) and physical mapping of *swh* (right). The *swh* genetically mapped to the most telomeric part of rat Chr17, 0.25-cM distal from *D17Rat132* and *D17Rat140*. In the physical map, the *swh* locus is localized to a ~0.2-Mb region between *D17Rat140* and the telomere. Both *Ero1lb* and *Edaradd* have been mapped within the *swh* locus. B, Sequence analysis of *Edaradd* gene of wild-type and *swh/swh* rats. In the genomic DNA of *swh/swh* rat, a C to T (red) transition is present in exon 6 of rat *Edaradd* gene. This changes proline to serine at codon 153 of the deduced EDARADD protein. Rat codon 153 corresponds to codon 156 of mouse EDARADD isoform 1 (NP_598398) and codon 153 human EDARADD isoform B (NP_542776). C, Amino-acid sequence alignment of a region of the EDARADD death domain from different species. The 153rd amino acid that is altered in *swh/swh* rat is highly conserved in the vertebrates.

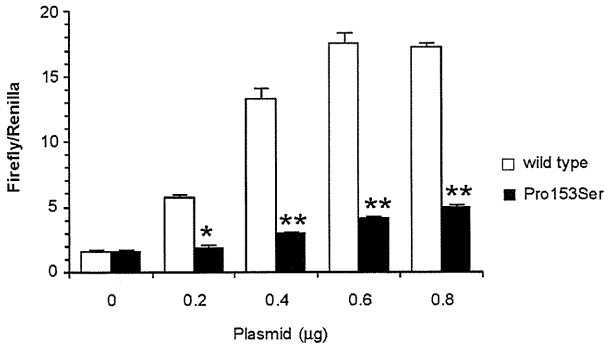

Figure 3 Loss of NF-κB activation by the Pro153Ser Edaradd mutant protein. 293T cells were transfected with 1.2 μg pNF-κB-luciferase reporter gene plasmid, 2 μg pRL-TK, and the amounts of each expression construct were measured in a reporter assay. The expression levels of luciferase were normalized to those of the internal control. Relative NF-κB activity in wild-type transfected cells increased in a dose-dependent manner, while significantly lower relative NF-κB activity was observed in the Pro153Ser *Edaradd*-transfected cells. *P < 0.01, **P < 0.001.

activated NF-κB in a dose-dependent manner. Meanwhile, Pro153Ser *Edaradd* showed significantly lower transcriptional activity of NF-κB than the wild type. The expression level of the Pro153Ser EDARADD protein detected by western blotting was not different from that of the wild type (data not shown). These findings indicate that the Pro153Ser missense mutation of the rat *Edaradd* gene could not activate NF-κB and that the Eda signaling pathway failed to function in *swh/swh* rats.

Discussion

In this study, we demonstrated that the *swh/swh* rat harbored a Pro153Ser mutation in the *Edaradd* gene and showed typical symptoms of HED, such as sparse hair, oligodontia, inability to sweat, and developmental defects of the ectoderm-derived glands [27]. Hence, we successfully established the *swh/swh* rat as a genetically and phenotypically well-characterized disease model of HED.

EDARADD is a 208 amino acid protein consisting of an N-terminal Tnf receptor-associated factor (Traf)-binding consensus sequence and a C-terminal death domain (DD). The Traf-binding consensus sequence of EDARADD is used as a docking site for Traf1, Traf2, and Traf3, thereby recruiting Traf members and leading eventually to the activation of NF-κB [6]. The DD is involved in self-association of EDARADD and its interaction with EDAR [6,25]. Thus, EDARADD is central to Edar signaling. The N-terminal region is responsible for signal transduction and the C-terminal DD is required for receptor engagement.

To date, four *EDARADD* mutations have been found in a subset of human HED, one leads to autosomal dominant inheritance (Leu112Arg) [26], while the others lead to autosomal recessive inheritance (Glu142Lys, Pro121Ser, and Thr135-Val136del) [6,28,29]. All of these mutations are located in the DD and functional analyses showed that they resulted in the failure of EDARADD to interact with EDAR and to activate NF-κB. In the *crinkled* mouse, a genomic region of ~66-kb or more which includes exon 6 that encodes the entire DD, is deleted [25]. The *crinkled* mouse displays developmental defects in hair follicles, teeth, and sweat glands [30,31]. Hence, it is possible that a mutation in the DD of EDARADD is necessary for the HED syndrome to be manifested both in human and mouse.

All members of the DD superfamily form a highly compact structure comprising six antiparallel α-helix that is involved in homotypic and heterotypic protein-protein complex formation [32]. The region spanning the α1 to α4 helices of the DD of MyD88, a member of the death receptor superfamily, is required for its interaction with a downstream kinase [33]. A comparison of the amino acid sequences of the DD superfamily revealed that the Pro153-Ser missense mutation found in the present study is located in the α4 helix of the DD of EDARADD. This mutation may cause a profound change in the polarity of a crucial region and eventually diminish NF-κB signaling. It is likely that Pro153Ser affects the structure of the DD thereby interfering in the interaction of EDARADD with EDAR.

Mutations affecting the Eda pathway are known in medaka [13], zebrafish [14], mouse [4,6,8], cattle [15-18], dog [19], and human [3,5,6]. Of them, the mouse mutants have been widely characterized as a model organism of HED. Here we report the *swh* mutation as the first example of a mutation in the Eda pathway in the rat.

Because the rat is closely related to the mouse, it is important to recognize how the rat *Edaradd* mutant phenotype matches the mouse Eda pathway mutant phenotypes. Similar to the mouse mutants, the *swh/swh* rat displayed sparse hair, misshapen teeth, and absence of sweating. Additionally, like the Eda pathway mutant, the *swh/swh* rat had only abnormal awl hair in the coat. The *swh/swh* rat showed a lack of the ectoderm-derived glands, meibomian, preputial, and tongue. Interestingly, both serous and mucous glands were absent in the tongue of the *swh/swh* rat. This is a clear difference from the mouse Eda pathway mutants that lacked mucous glands but had serous glands in the tongue [34]. Moreover, in contrast to the complete absence of tail hair in the Eda pathway mutant mice, the *swh/swh* rat had hair on its tail. The penetrance of the kink tail phenotype was low in the *swh/swh* rat, while almost all Eda pathway mutant mice showed the kink tail. Lastly, the bald patch behind the ear was not present in the *swh/swh* rat, although it was a very characteristic phenotype of the Eda pathway mutant mice.

Why these phenotypes are different between the Eda pathway mutant mice and the *swh/swh* rats is yet to be explained. However, different types of mutations could possibly explain the differences. The mouse *crinkled* mutation is a deletion [6], while the *swh* mutation is missense. Although the Luc-reporter assay strongly suggested that *swh* is a null mutation, the possibility that *swh* might be a hypomorphic mutation cannot be eliminated because the activation of NF-κB found in the assay was very low. In the Eda pathway mutant mice, the mammary, salivary and tracheal submucosal glands have been well characterized [9,10]. Further analyses of these glands in *swh/swh* rats will give further insights into the functions of the Eda pathway genes in the development of these glands.

Conclusions

We successfully established the *swh/swh* rat as the first rat model of HED and identified *swh* as a Pro135Ser missense mutation in the *Edaradd* gene. The Pro135Ser mutant protein failed to activate NF-κB in the Eda signaling pathway. Thus, the *swh/swh* rat is a good model that can be used to investigate the pathological basis of HED.

Acknowledgements and Funding

The authors are grateful to the National BioResource Project for the Rat for providing the ACI/NKyo, WTC/Kyo, and WTC-*swh*/Kyo rat strains. This work was supported in part by the Grants-in-aid for Scientific Research from the Japan Society for the Promotion of Science (21300153 to TK) and by a Grant-in-aid for Cancer Research from the Ministry of Health, Labour and Welfare (to TK).

Authors' contributions

TK and MY performed the genetic and molecular biological experiments. RH and HH performed the histological examinations. TK wrote the paper and HH and TS revised the manuscript. All authors read and approved the final manuscript.

Received: 29 July 2011 Accepted: 21 October 2011
Published: 21 October 2011

References

1. Mikkola ML, Thesleff I: **Ectodysplasin signaling in development.** *Cytokine Growth Factor Rev* 2003, **14(3-4)**:211-224.
2. Salisbury DM, Stothers JK: **Hypohidrotic ectodermal dysplasia and sudden infant death.** *Lancet* 1981, **1(8212)**:153-154.
3. Kere J, Srivastava AK, Montonen O, Zonana J, Thomas N, Ferguson B, Munoz F, Morgan D, Clarke A, Baybayan P, *et al*: **X-linked anhidrotic (hypohidrotic) ectodermal dysplasia is caused by mutation in a novel transmembrane protein.** *Nat Genet* 1996, **13(4)**:409-416.
4. Srivastava AK, Pispa J, Hartung AJ, Du Y, Ezer S, Jenks T, Shimada T, Pekkanen M, Mikkola ML, Ko MS, *et al*: **The Tabby phenotype is caused by mutation in a mouse homologue of the *EDA* gene that reveals novel mouse and human exons and encodes a protein (ectodysplasin-A) with collagenous domains.** *Proc Natl Acad Sci USA* 1997, **94(24)**:13069-13074.
5. Monreal AW, Ferguson BM, Headon DJ, Street SL, Overbeek PA, Zonana J: **Mutations in the human homologue of mouse dl cause autosomal recessive and dominant hypohidrotic ectodermal dysplasia.** *Nat Genet* 1999, **22(4)**:366-369.
6. Headon DJ, Emmal SA, Ferguson BM, Tucker AS, Justice MJ, Sharpe PT, Zonana J, Overbeek PA: **Gene defect in ectodermal dysplasia implicates a death domain adapter in development.** *Nature* 2001, **414(6866)**:913-916.
7. Mikkola ML: **Molecular aspects of hypohidrotic ectodermal dysplasia.** *Am J Med Genet A* 2009, **149A(9)**:2031-2036.
8. Headon DJ, Overbeek PA: **Involvement of a novel Tnf receptor homologue in hair follicle induction.** *Nat Genet* 1999, **22(4)**:370-374.
9. Chang SH, Jobling S, Brennan K, Headon DJ: **Enhanced Edar signalling has pleiotropic effects on craniofacial and cutaneous glands.** *PLoS One* 2009, **4(10)**:e7591.
10. Melnick M, Phair RD, Lapidot SA, Jaskoll T: **Salivary gland branching morphogenesis: a quantitative systems analysis of the Eda/Edar/NFκB paradigm.** *BMC Dev Biol* 2009, **9**:32.
11. Gruneberg H: **The glandular aspects of the tabby syndrome in the mouse.** *J Embryol Exp Morphol* 1971, **25(1)**:1-19.
12. Gaide O, Schneider P: **Permanent correction of an inherited ectodermal dysplasia with recombinant EDA.** *Nat Med* 2003, **9(5)**:614-618.
13. Kondo S, Kuwahara Y, Kondo M, Naruse K, Mitani H, Wakamatsu Y, Ozato K, Asakawa S, Shimizu N, Shima A: **The medaka *rs-3* locus required for scale development encodes ectodysplasin-A receptor.** *Curr Biol* 2001, **11(15)**:1202-1206.
14. Harris MP, Rohner N, Schwarz H, Perathoner S, Konstantinidis P, Nusslein-Volhard C: **Zebrafish eda and edar mutants reveal conserved and ancestral roles of ectodysplasin signaling in vertebrates.** *PLoS Genet* 2008, **4(10)**:e1000206.
15. Drogemuller C, Distl O, Leeb T: **Partial deletion of the bovine *ED1* gene causes anhidrotic ectodermal dysplasia in cattle.** *Genome Res* 2001, **11(10)**:1699-1705.
16. Drogemuller C, Peters M, Pohlenz J, Distl O, Leeb T: **A single point mutation within the *ED1* gene disrupts correct splicing at two different splice sites and leads to anhidrotic ectodermal dysplasia in cattle.** *J Mol Med (Berl)* 2002, **80(5)**:319-323.
17. Ogino A, Kohama N, Ishikawa S, Tomita K, Nonaka S, Shimizu K, Tanabe Y, Okawa H, Morita M: **A novel mutation of the bovine *EDA* gene associated with anhidrotic ectodermal dysplasia in Holstein cattle.** *Hereditas* 2011, **148(1)**:46-49.
18. Gargani M, Valentini A, Pariset L: **A novel point mutation within the *EDA* gene causes an exon dropping in mature RNA in Holstein Friesian cattle breed affected by X-linked anhidrotic ectodermal dysplasia.** *BMC Vet Res* 2011, **7**:35.
19. Casal ML, Scheidt JL, Rhodes JL, Henthorn PS, Werner P: **Mutation identification in a canine model of X-linked ectodermal dysplasia.** *Mamm Genome* 2005, **16(7)**:524-531.
20. Kuramoto T, Morimura K, Nomoto T, Namiki C, Hamada S, Fukushima S, Sugimura T, Serikawa T, Ushijima T: **Sparse and wavy hair: a new model for hypoplasia of hair follicle and mammary glands on rat chromosome 17.** *J Hered* 2005, **96(4)**:339-345.
21. Saar K, Beck A, Bihoreau MT, Birney E, Brocklebank D, Chen Y, Cuppen E, Demonchy S, Dopazo J, Flicek P, *et al*: **SNP and haplotype mapping for genetic analysis in the rat.** *Nat Genet* 2008, **40(5)**:560-566.
22. Rothschild TC, Boylan ES, Calhoon RE, Vonderhaar BK: **Transplacental effects of diethylstilbestrol on mammary development and tumorigenesis in female ACI rats.** *Cancer Res* 1987, **47(16)**:4508-4516.
23. Kuramoto T, Kuwamura M, Tokuda S, Izawa T, Nakane Y, Kitada K, Akao M, Guenet JL, Serikawa T: **A mutation in the gene encoding mitochondrial Mg^{2+} channel MRS2 results in demyelination in the rat.** *PLoS Genet* 2011, **7(1)**:e1001262.
24. Reed WB, Lopez DA, Landing B: **Clinical spectrum of anhidrotic ectodermal dysplasia.** *Arch Dermatol* 1970, **102(2)**:134-143.
25. Yan M, Zhang Z, Brady JR, Schilbach S, Fairbrother WJ, Dixit VM: **Identification of a novel death domain-containing adaptor molecule for ectodysplasin-A receptor that is mutated in crinkled mice.** *Curr Biol* 2002, **12(5)**:409-413.
26. Bal E, Baala L, Cluzeau C, El Kerch F, Ouldim K, Hadj-Rabia S, Bodemer C, Munnich A, Courtois G, Sefiani A, *et al*: **Autosomal dominant anhidrotic ectodermal dysplasias at the EDARADD locus.** *Hum Mutat* 2007, **28(7)**:703-709.
27. Pispa J, Thesleff I: **Mechanisms of ectodermal organogenesis.** *Dev Biol* 2003, **262(2)**:195-205.
28. Chassaing N, Cluzeau C, Bal E, Guigue P, Vincent MC, Viot G, Ginisty D, Munnich A, Smahi A, Calvas P: **Mutations in *EDARADD* account for a small proportion of hypohidrotic ectodermal dysplasia cases.** *Br J Dermatol* 2010, **162(5)**:1044-1048.
29. Suda N, Bazar A, Bold O, Jigjid B, Garidkhuu A, Ganburged G, Moriyama K: **A Mongolian patient with hypohidrotic ectodermal dysplasia with a novel P121S variant in *EDARADD*.** *Orthod Craniofac Res* 2010, **13(2)**:114-117.

30. Kindred B: **The expression of the Tabby and crinkled genes in different genetic backgrounds in the mouse.** *Genetics* 1967, **55(1)**:173-178.
31. Rao MS, Jaszczak E, Landis SC: **Innervation of footpads of normal and mutant mice lacking sweat glands.** *J Comp Neurol* 1994, **346(4)**:613-625.
32. Weber CH, Vincenz C: **The death domain superfamily: a tale of two interfaces?** *Trends Biochem Sci* 2001, **26(8)**:475-481.
33. Loiarro M, Gallo G, Fanto N, De Santis R, Carminati P, Ruggiero V, Sette C: **Identification of critical residues of the MyD88 death domain involved in the recruitment of downstream kinases.** *J Biol Chem* 2009, **284(41)**:28093-28103.
34. Wells KL, Mou C, Headon DJ, Tucker AS: **Defects and rescue of the minor salivary glands in Eda pathway mutants.** *Dev Biol* 2011, **349(2)**:137-146.

doi:10.1186/1471-2156-12-91
Cite this article as: Kuramoto *et al.*: A rat model of hypohidrotic ectodermal dysplasia carries a missense mutation in the *Edaradd* gene. *BMC Genetics* 2011 **12**:91.

Brain Research Bulletin 86 (2011) 36–41

Contents lists available at ScienceDirect

Brain Research Bulletin

journal homepage: www.elsevier.com/locate/brainresbull

Research report

Neuroprotective effect of levetiracetam on hippocampal sclerosis-like change in spontaneously epileptic rats

Sei Sugata[a], Ryosuke Hanaya[a,*], Kenta Kumafuji[b], Mai Tokudome[a], Tadao Serikawa[b], Kaoru Kurisu[c], Kazunori Arita[a], Masashi Sasa[d]

[a] Department of Neurosurgery, Graduate School of Medical and Dental Sciences, Kagoshima University, Kagoshima 890-8544, Japan
[b] Institute of Laboratory Animals, Graduate School of Medicine, Kyoto University, Kyoto 606-8501, Japan
[c] Department of Neurosurgery, Graduate School of Biomedical Sciences, Hiroshima University, Hiroshima 734-8551, Japan
[d] Nagisa Clinic, Hirakata 573-1183, Japan

ARTICLE INFO

Article history:
Received 6 April 2011
Received in revised form 16 May 2011
Accepted 30 May 2011
Available online 6 June 2011

Keywords:
Levetiracetam
Neuroprotection
Spontaneous epileptic rat (SER)
Hippocampal cell loss
Mossy fiber sprouting
Brain-derived neurotrophic factor (BDNF)

ABSTRACT

The spontaneously epileptic rat (SER) begins to exhibit both tonic convulsions and absence seizures from 6 weeks of age and SERs have stable seizures after 10 weeks of age. Low-dose administrations of levetiracetam (LEV) for 4- to 5-weeks-old SERs which did not show spontaneous seizures reduced both seizures 5 weeks after termination of administration. The hippocampus of SER exhibited decreased CA3 neurons, sprouting of mossy fibers, and hyperexpression of the brain-derived neurotrophic factor (BDNF). We attempted prophylactic LEV administrations in preseizure-manifesting SERs to evaluate if such a treatment regimen would protect the hippocampal sclerosis-like changes observed in SERs. The osmotic mini-pump administered LEV dissolved in saline to 4-weeks-old SERs for 4 weeks at 2.5 μl/h. LEV was administered at 420 mg/ml for 4 weeks in Group A. In Group B, LEV was given at 420 mg/ml for the first 2 weeks followed by doubling the dosage (840 mg/ml) in the following 2 weeks. LEV administrations in preseizure-manifesting SERs reduced the decrease of CA3 neurons and mossy fibers sprouting at 10–11 weeks of age in both group A and B. LEV attenuated BDNF expression in inner molecular layers of the dentate gyrus, striatum radiatum, and CA3 in 10- to 11- and 14- to 15-weeks-old SERs. In group B, LEV decreased BDNF expression in hilus and CA1 of 10- to 11- weeks-old SER. The present results suggest that prophylactic treatment with LEV in preseizure-manifesting SERs inhibits hippocampal sclerosis-like neuronal degeneration and/or regeneration.

1. Introduction

Levetiracetam (LEV) is a pyrrolidone derivative structurally related to piracetam [6], and the chemical structure is different from other currently available antiepileptic agents. LEV is extensively used for partial and/or generalized epilepsy since 2002 [17,24]. LEV shows a unique, antiepileptic profile and recent findings have revealed that LEV binds to SV2A protein, which presumably is involved in regulating neurotransmitter release [28]. During the process of epileptogenesis, manifestations of certain characteristic histological changes, including neuronal death/loss and neurogenesis leading to reorganization of cell membrane matrixes and formation of axonal/dendritic sprouting and gliosis, are obvious [34]. In fact, cellular network alterations composed of neuronal loss, axonal sprouting, gliosis and reorganization of neuronal circuits have been demonstrated [21,47]. However, there are some reports showing that LEV may have a neuroprotective effect against epileptogenesis: LEV exhibits neuroprotective effects on kinic acid-induced toxicity [30] and stroke and head injuries in an experimental model [11,43].

Thus, in an attempt to elucidate whether LEV elicited an antiepileptogenic activity, the effects of LEV on neuronal loss, sprouting and brain derived neurotrophic factor (BDNF) expression were examined using SERs in this study. The SER (*zi/zi, tm/tm*) is a double mutant obtained by mating heterozygous tremor rats (*tm/+*), a mutant found in an inbred colony of Kyoto-Wistar rats [44], with homozygous zitter rats (*zi/zi*) found in a Sprague-Dawley colony [36]. SERs at 6 weeks (wk) of age begin to spontaneously show tonic convulsion and absence seizures. The seizures increase in accordance with aging, and frequency and duration of the seizures did not have age-related differences in SER after 10 wk of age [40]. Each seizure was characterized by low voltage fast waves and 5–7 Hz spike-wave-like seizures in cortical and hippocampal EEG, respectively [37,39]. The antiepileptic profiles of conventional antiepileptic drugs on SER parallel those in human epilepsy [37]. We

* Corresponding author at: Department of Neurosurgery, Graduate School of Medical and Dental Sciences, Kagoshima University, 8-35-1 Sakuragaoka, Kagoshima 890-8544, Japan. Tel.: +81 99 275 5375; fax: +81 99 265 4041.
E-mail address: hanaya@m2.kufm.kagoshima-u.ac.jp (R. Hanaya).

0361-9230/$ – see front matter © 2011 Elsevier Inc. All rights reserved.
doi:10.1016/j.brainresbull.2011.05.017

have reported that hippocampal CA3 pyramidal neurons in SERs show a long-lasting depolarizing shift accompanied by repetitive firing with a single stimulation of the mossy fibers [12], and this abnormal excitability is attributable to abnormalities of the L-type Ca^{2+} channels [46]. Morphological studies have demonstrated a decrease in the number of CA3 neurons with maturation, sprouting of mossy fiber in the dentate, and BDNF hyperexpression along the mossy fiber (MF) in a manner analogous to hippocampal sclerosis in complex partial seizures [10].

Here we examined if prophylactic administration of LEV in preseizure-manifesting SERs would protect the hippocampal sclerosis-like change occurred in mature SERs that exhibit tonic convulsion and absence seizures.

2. Materials and methods

2.1. Experimental animals

A total 36 SERs of both sexes at 4 wk of age (prior to manifestation of epileptic seizures) were implanted with an osmotic mini-pump (Alzet, Cupertino, USA) each under the skin at the back for LEV administration. The osmotic mini-pump administered LEV (previously dissolved in physiological saline) or saline alone (controls) for 4 wk at 2.5 μl/h. In Groups A and B, LEV at 420 mg/ml or saline was administered for 4 wk, respectively. To maintain a consistent therapeutic concentration in the animals (10–100 μM), a specific administration regimen was employed [15]: LEV was given at 420 mg/ml for the first 2 wk followed by 840 mg/ml for the subsequent 2 wk, taking into consideration of SER growth in Group B. All animals were kept in individual cages in a room maintained at 23 ± 2 °C and 55 ± 5% relative humidity, and were provided with standard rat chow (MF, Oriental Yeast, Tokyo) and tap water ad libitum. We measured serum LEV concentration at 6- and 8-wk of age. Under ether anesthesia, we took 0.3 ml-blood sample from SER. Serum sample obtained from blood centrifugation (1500 × g, 15 min) was frozen to −20 °C and sent Mitsubishi Chemical Medience Corporation (Tokyo) to measure LEV concentration. Serum LEV was analyzed by gas chromatography/mass spectrometry methods. At 10–11 and 14–15 wk of age, SERs were euthanized with 60 mg/kg sodium pentobarbital. Monitoring regimen was scheduled as described in Fig. 1. Brains of sacrificed animals were isolated and sectioned with the right hemispheres for cell count and BDNF staining, while the left hemispheres were subjected to Timm's staining in the middle after removal and washing in ice-cold saline. All treatment until brain fixation was operated in Hiroshima University. Histological examination using fixed brain was performed in Hiroshima University and Kagoshima University.

2.2. Cell count

After fixation (in 4% paraformaldehyde in 0.1 M phosphate buffer (PB) at pH 7.4) at 4 °C, brains were embedded in paraffin and 4-μm-thick coronal sections were sliced from the anterior to the posterior level. The anteroposterior sections were appropriated according to stereotaxic coordinates of the rat [33]. After hematoxylin-eosin staining, quantification of cell density of coronal sections was performed with a 10 × 10 box with 1 cm^2 microscopic grid. The grid for counting was placed on a well-defined area of the cerebral structure of interest, and counting was carried out with a microscopic enlargement of 200- and 400-fold specifically defined for the respective structures.

Cell counting was performed twice on serial three adjacent sections for each investigated region by a single unbiased observer. Cell counts obtained in every counted field of the 3 sections were pooled and the mean was derived. This procedure was used to minimize potential errors resulting from double-counting. Neurons touching the inferior and edges of the grid were not counted. Counts involved only neurons with cell body larger than 10 μm diameter. Cells with small cell body were considered as glial cells and were not counted.

2.3. Timm's staining

After treatment in 0.1 mol/l PB containing 0.16% Na_2S (pH 7.3) for 1 h, brains were fixed in 0.1 mol/l PB containing 3% glutaraldehyde and 0.16% Na_2S for 1 day before further fixation in 15% sucrose solution for 2 days. The brains were frozen, and cut into 20 μm sagittal sections with a microtome. The sections were mounted on slides and developed in a solution containing 75 ml of 20% gum arabic, 15 ml of a 2% hydroquinone and 3% citric acid mixture, and 1.5 ml of 10% silver nitrate, in the dark for about 1 h. The reaction was terminated by immersing the brain slices in 5% sodium thiosulphate.

2.4. Immunohistochemistry

Tissue sections (thickness: 4 μm) were deparaffinized with xylene, and antigen was harvested with the heat-induced epitope retrieval method using citrate buffer solution (pH 6.0). Degrading effects of endogenous peroxidase were inhibited by dipping the slides into a solution containing a mixture of 30% H_2O_2 (10 ml) and 99% methanol (90 ml) for 30 min. The treated slides were then rinsed and serially washed with 0.01 M phosphate buffered saline (PBS, pH 7.4); 3–5 min were allocated for each washing. An indirect method for immunostaining the antibody, or the labeled streptavidin biotin (SAB) method using Histofine simple stain (Nichirei Company. Tokyo, Japan), was performed with rabbit polyclonal anti-BDNF antibodies (1:100, Dako-Cytomation). Primary antibody incubation was performed overnight at 4 °C, followed by 30-min incubation with secondary antibodies (biotinylated secondary antibodies, SAB kit; Nichirei Company). The reaction mixture was further incubated for 5–10 min with 0.02% diaminobenzidine (DAB tablet; Wako Pure Chemical Industry, Osaka, Japan) and 0.05% H_2O_2 in PBS. All slides were each mounted with a coverslip for storage. Immunohistochemical control sections from two animals underwent similar above-mentioned procedures for all antibodies except for exposure to the primary antibodies.

2.5. Densitometric analysis of immunoreactivity

Images captured by a 3-CCD color video camera (DP 70; Olympus, Tokyo, Japan) mounted on a light microscope (BH 2; Olympus) were relayed to a video monitor and a computer equipped with imaging software (DPC controller, Olympus). The areas of interest selected from the sections and the optical density (OD) of each region (demarcated according to the rat brain atlas) were measured blind by a reader. Images of all areas of interest were captured at 40× or 100× magnification. The color images were transformed to black and white images and analyzed accordingly (Image J software; NIH, USA). Immunoreactivity was expressed as OD. Standard transfer curves of the gray level produced by filters of known OD (Kodak, New York, USA) were used for calibration. The mean value of serial 3 sections in each area was calculated. Each value was derived from the difference between the value of region-of-interest and that of white matter of parietal cortex. Each value was corrected to the fourth decimal place.

2.6. Statistical analysis

The values obtained in levetiram-treated SERs were compared with those of saline-treated SER. Group comparisons were determined initially by analysis of variance (ANOVA) for independent groups followed by the Fischer's test.

3. Results

3.1. Serum LEV concentration

Serum LEV concentrations, which were monitored at ages of 6- and 8-wk before operation using the immunofluorescence method, registered 29.1 ± 3.6 and 34.4 ± 3.3 μg/ml in 6- (groups A and B) and 8- (group B) wk-old SERs, respectively. In group A, the LEV concentrations decreased to 18.3 ± 1.1 μg/ml at 8-wk-old. All SERs indicated therapeutic concentrations (10–100 μM) [15] of LEV throughout the prophylactic administration period.

3.2. Hippocampal neurons

The number of CA3 neurons in 14- to 15-wk-old SERs of physiological saline (PS)-treated group B control was significantly ($p < 0.01$) lower (20.7 ± 2.1) than those in 10- to 11-wk-old SERs of groups A control (24.5 ± 2.5) and B control (24.7 ± 1.4). The neuronal counts were comparable to our previous results [10], where surgical intervention did not affect the hippocampal neurons. LEV significantly ($p < 0.01$) inhibited the decreases of CA3 neurons in 10- to 11-wk-old SERs of both groups A (29.5 ± 1.2) and B (30.5 ± 2.5). However, the inhibitory effect was not significantly observed in 14- to 15-wk-old SERs (21.3 ± 2.5), when it was 6 wk after termination of LEV administration (Fig. 2, Table 1).

3.3. Sprouting of mossy fiber in the dentate gyrus

The extent of sprouting was ranked according to the sprouting scores [3]. Sprouting of MF was observed in the inner molecular layer of the dentate gyrus in all PS-treated SERs. Operative effects did not affect MF-sprouting in 14- to 15-wk-old SERs, a finding which is compared with our previous report [10]. In PS treated group, the sprouting scores were higher in SER of group B control

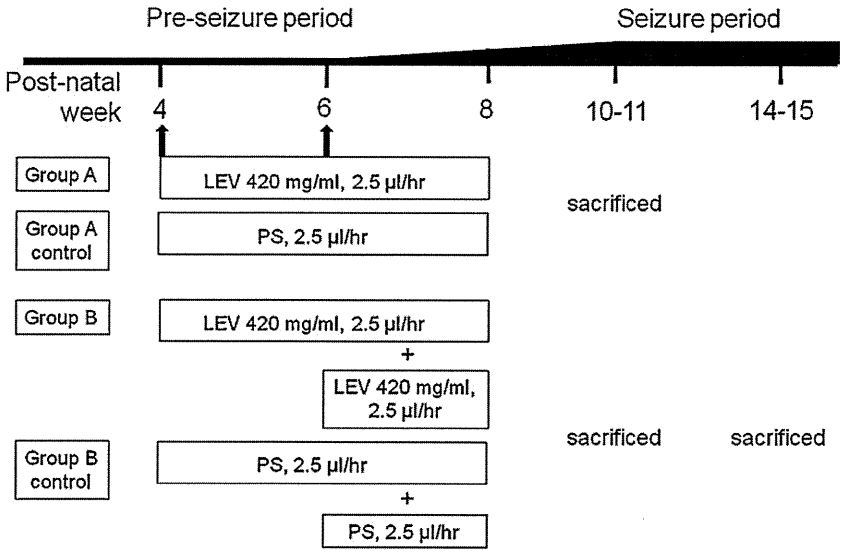

Fig. 1. Regimen for placebo and levetiracetam (LEV) administration: an osmotic mini-pump was embedded in the dorsal skin of each animal, and placebo (physiological saline: PS) or LEV was subcutaneously delivered at a rate of 2.5 µl/h. To maintain a consistent therapeutic concentration in the animals (10–100 µM), the dosage was doubled in the later 2 of the 4-weeks regimen. Refer to details in Section 2.1.

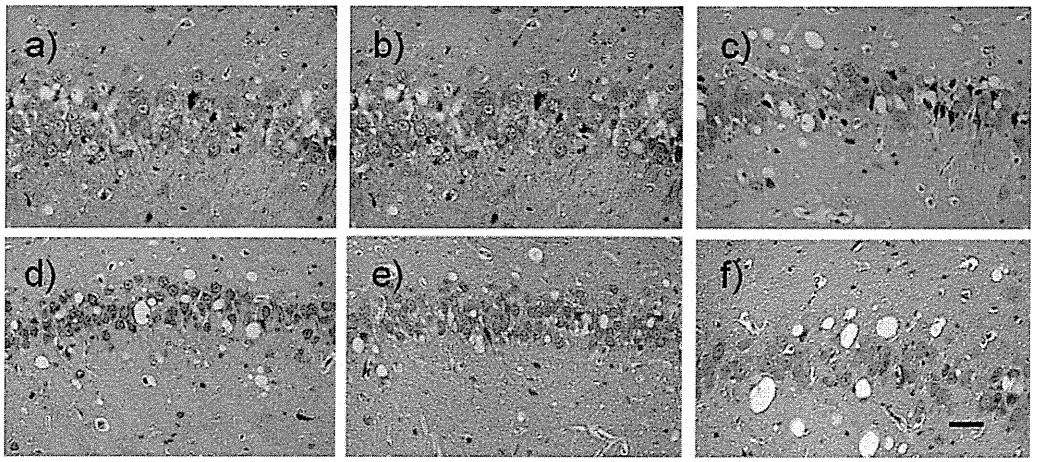

Fig. 2. Effects of levetiracetam on CA3 pyramidal neuron in spontaneously epileptic rat: Groups A, B (10- to 11-weeks-old) and B (14 to 15-weeks-old) were treated with each placebo (a, b, c) or levetiracetam (d, e, f). Number of CA3 neurons in each placebo was less at 14- to 15-weeks-old (c) than at 10- to 11-weeks-old (a, b). Levetiracetam inhibited CA3 neuronal loss at 10- to 11-weeks-old (d, e), but not at 14- to 15-weeks-old (f). Scale bar: 50 µm.

(2.8 ± 1.0) at 14–15 wk of age than those found in groups A control (1.4 ± 0.5) and B control (1.6 ± 0.6) at 10–11 wk of age. LEV significantly ($p < 0.01$) reduced MF sprouting in 10- to 11-wk-old SERs of group B (0.5 ± 0.5), compared with group B control; however this was not the case in group A (1.0 ± 0.6) versus group A control (1.4 ± 0.5). In 14- to 15-wk-old SERs, LEV did not reduce MF scores in group B (2.8 ± 1.0) compared to group B control (3.0 ± 0.9) (Fig. 3, Table 1).

Table 1
Numbers of hippocampal CA3 neurons and Sprouting score of mossy fiber in SERs.

Ages (weeks)	Numeber of neurons		Sprouting score of mossy fiber	
	10–11	14–15	10–11	14–15
Group A				
LEV	29.5 ± 1.2#		1.0 ± 0.6	
Control	24.5 ± 2.5		1.4 ± 0.5	
Group B				
LEV	30.5 ± 2.5#	21.3 ± 2.5	0.5 ± 0.5#	2.8 ± 1.0
Control	24.7 ± 1.4	20.7 ± 2.1	1.6 ± 0.6	3.0 ± 0.9

Average ± S.D.
Control: physiological saline-treated SERs in both group A and group B.
LEV: levetiracetam-treated SERs.
# $p < 0.01$ compared to each physiological saline-treated group.

3.4. Immunoreactivity of BDNF

Analysis of BDNF immunoreactivity (expressed as the optical) was performed after correction for background density. The densitometry levels of BDNF immunoreactivity were higher in the stratum radiatum, pyramidal layer, stratum oriens of CA3, and supragranular layer of the dentate gyrus in 14- to 15-wk-old SERs than those in 10- to 11-wk-old SERs of groups A control and B control. In 10- to 11-wk-old SERs, LEV significantly ($p < 0.05$) reduced BDNF expression in the CA3 pyramidal layer, stratum ratiatum and supragranular layer of the dentate gyrus. LEV given at the higher dose in 10- to 11-wk-old SERs also suppressed BDNF expression in the hilus, granular and inner molecular layer of the dentate gyrus (Fig. 4), CA1 and stratum radiatum. In 14- to 15-wk-old SERs, the significantly inhibitory effects of LEV were still observed except for the CA1, albeit insignificant effects were noted in the hilus and CA1

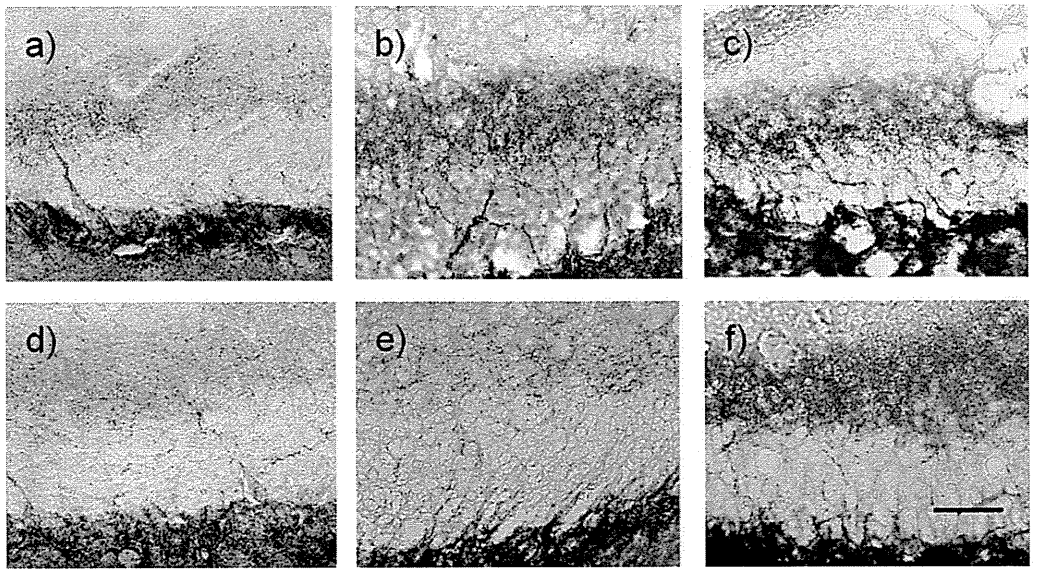

Fig. 3. Effect of levetiracetam on mossy-fiber sprouting in spontaneously epileptic rat: In placebo-treated SER, Timm's staining of the dentate gyrus revealed obvious sprouting in groups A (a) and B (b) at 10- to 11-weeks-old, and B (c) at 14- to 15-weeks-old. Mossy fiber sprouting in each placebo was increased with age (a, b < c). Levetiracetam inhibited mossy-fiber sprouting in both group A and B (d, e) at 10- to 11-weeks-old, but not in group B at 14- to 15-weeks-old (f). Scale bar: 50 μm.

areas (note that, BDNF expression tended to decrease in these areas; Table 2).

4. Discussion

4.1. Profile of levetiracetam

LEV shows a unique, antiepileptic profile: it inhibits seizures in amygdale- and pentylentetrazole-kindled animals [19,26,32] as well as epileptic seizures in genetic epilepsy model animals without affecting acute maximal electroshock or pentylentetrazole-induced seizures. LEV inhibits absence seizures in genetic absence epilepsy rats from Strasbourg (GAERS), groggy rats and spontaneously epileptic rats (SERs) as well as convulsive seizures in audiogenic-seizure sensitive rats [7,14,41].

The antiepileptic mechanisms of action are also completely different from those of the conventional and other newly available antiepileptic drugs: (i) LEV has no effects on voltage-gated ion channels (such as the Na^+, K^+ or Ca^{2+} channels), except for the N-type Ca^{2+} channel [2,4,5,27,48]; and (ii) LEV does not affect the neurotransmitter-related receptors such as glutamate or $GABA_{A/B}$ receptors [20,29]. LEV binds to SV2A protein, which presumably is involved in regulating neurotransmitter release [28]. The antiepileptic action of LEV has been demonstrated to involve SV2A binding, since the inhibitory effect of LEV on seizures induced by 6-Hz electric pulse stimulation is induced in one-half of heterozygous SV2A(+/−) mice and wild-type SV2A(+/+) mice, although SV2A knock-out mice manifest convulsion and die before 2 wk of age [16].

LEV is considered to have some antiepileptogenic effects, since continuous LEV administration during the kindling process inhibits development of both amygdale- and PTZ-kindling as well as kindling in hippocampal kindling Noda epileptic rats (NERs), and genetic epilepsy model animals [13,19,26,32]. Similar results have been reported in the audiogenic kindling model [42]. In addition, our previous study has showed that daily LEV injections in preseizure-manifesting rats (from 4 to 8 wk of age) inhibit the incidence of

Table 2
Expression of BDNF in hippocampus of both physiological saline- and levetiracetam-treated SERs.

	10–11 weeks of age				14–15 weeks of age	
	Control (A)	LEV (A)	Control (B)	LEV (B)	Control (B)	LEV (B)
CA1						
Pyramidal layer	5.5 ± 0.8	5.2 ± 2.6	5.6 ± 0.7	3.5 ± 0.6*	6.3 ± 2.1	6.4 ± 0.7
S. oriens	5.2 ± 2.5	5.2 ± 1.0	5.4 ± 1.0	3.2 ± 0.5*	6.8 ± 1.9	6.5 ± 0.9
CA3						
Pyramidal layer	8.3 ± 1.1	4.6 ± 1.6*	8.1 ± 2.0	2.9 ± 1.3#	9.9 ± 3.9‡	5.2 ± 1.6#
S. oriens	5.1 ± 1.8	4.1 ± 1.4	5.6 ± 1.1	3.4 ± 0.9*	9.0 ± 4.0‡	6.1 ± 1.5*
Hilus	7.2 ± 1.1	6.4 ± 3.7	6.9 ± 1.6	3.0 ± 1.6*	7.3 ± 2.1	3.5 ± 1.9#
S. radiatum	4.4 ± 2.5	2.9 ± 2.2*	4.3 ± 2.5	2.7 ± 1.0*	9.3 ± 3.2‡	4.8 ± 2.9#
Dentate gyrus						
Granular layer	6.8 ± 1.4	4.1 ± 1.0	6.7 ± 1.3	2.7 ± 1.0#	6.8 ± 0.6	4.1 ± 0.9*
IML: sgl	8.3 ± 1.0	5.8 ± 2.0*	8.4 ± 0.1	3.8 ± 0.7#	10.3 ± 1.0‡	5.8 ± 1.0#
IML: outer part	6.0 ± 2.5	4.4 ± 1.2	5.7 ± 2.1	2.5 ± 0.5*	7.7 ± 2.1	5.7 ± 1.2
OML: inner part	4.8 ± 1.3	5.3 ± 0.9	4.8 ± 1.9	3.8 ± 0.8	5.2 ± 1.2	5.4 ± 0.8
OML: outer part	5.2 ± 2.2	5.0 ± 1.4	4.7 ± 1.5	3.5 ± 1.0	5.1 ± 1.3	5.3 ± 0.8

Average ± S.D. ($\times 10^{-3}$).
Control: physiological saline-treated SERs, LEV: levetiracetam-treated SER in both group A and group B, IML: inner molecular layer, OML: outer molecular layer, sgl: suragranular layer.
* $p < 0.05$ compared to each physiological saline-treated group.
# $p < 0.01$ compared to each physiological saline-treated group.
‡ $p < 0.05$ compared to physiological saline-treated SERs at 10- to 11-weeks-old in both group A and group B.

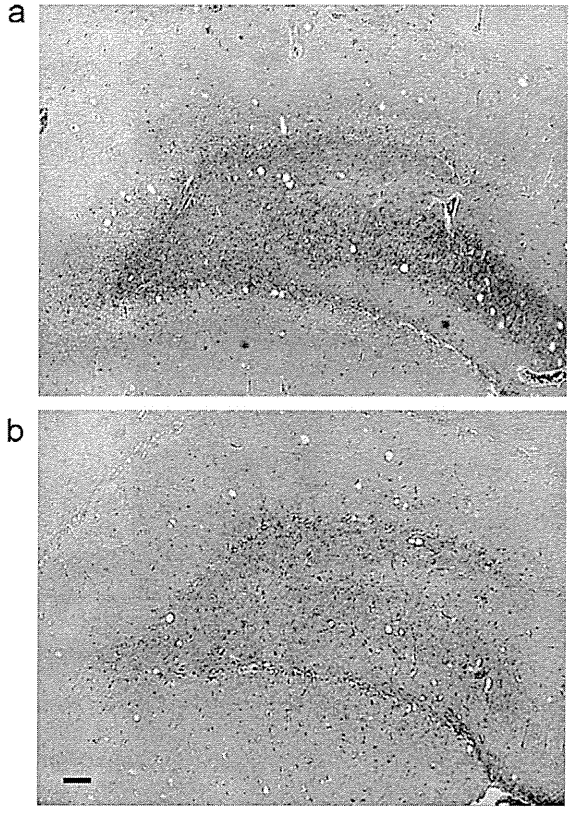

Fig. 4. Effect of levetiracetam on BDNF expression in dentate gyrus of spontaneously epileptic rat: In group B at 10- to 11-weeks-old, levetiracetam-treated SER (b) exhibited less BDNF expression than placebo-treated SER (a) in hilus, granular layer, and inner molecular layer of dentate gyrus. Scale bar: 200 μm.

seizures after 8-wk-old [45]. Epileptogenesis is gradually and progressively formed after establishment of an epileptic focus and progresses with more frequent and repeated seizures [25,38]. Epileptogenesis is gradual after establishment of an epileptic focus and progresses with repeated seizures. During this developmental process, histological changes, such as neuronal loss and neurogenesis, result in reorganization of cell matrixes and axonal/dendritic sprouting [34].

4.2. Neuroprotective effect of levetiracetam in spontaneously epileptic rats

In SERs, which spontaneously exhibit absence-like seizures and convulsive seizures 8–10 wk after birth, a decrease in the number of hippocampal CA3 neurons with age results in repeated seizures [10]. In addition, sprouting reflecting neurogenesis is detected in the inner molecular layer of dentate with age; a phenomenon analogous to neuronal loss. These findings in the genetic epileptic SER coincide well with those in kindling animals [3,35]. Furthermore, in tandem with neuronal loss and sprouting, BDNF expression was enhanced in the hippocampal CA3 pyramidal layer, hilus and granular layer of the dentate gyrus with age. This finding also concurs with that in kindling animal [3,31]. The progressive reorganization of neuronal circuits including neuronal loss, axonal sprouting and gliosis has been reported in human epilepsy [47]. Epileptogenesis in SERs is considered to have been induced at premature ages and by repeated seizures, although SERs are originally devoid of the aspertoacetylase-encoding genes that regulate the metabolism of N-acetyl-L-aspartate (NAA) to form acetate and aspartate [18] and of attractin for myeline formation [23].

Three to 6 wk after termination of 4-wk LEV administration before seizure manifestation, prevention of neuronal loss and inhibition of increased BDNF as well as sprouting were observed in the dentate areas. The increased NAA in SER hippocampus acts on the metabotropic glutamate receptors to induce excessive influxes of Na^+ and Ca^{2+} into CA3 neurons [9,46]. In addition, abnormalities of L-type Ca^{2+} channels in SER hippocampal CA3 neurons, such as lower thresholds for channel-opening and delayed inactivation, induce excessive Ca^{2+} influxes into CA3 neurons [1,46]. The SER CA3 neurons are hypersensitive to glutamate: i.e. glutamate receptor-linked cation channels show a lower opening threshold [8]. All these events are considered to be involved in neuronal death in SER hippocampus, and in turn, induce a compensatory BDNF increase to prevent neuronal death. BDNF is reported to induce hyperexcitable reentrant circuits in the dentate gyrus [22]. It is also likely that the increased BDNF has contributed to induction of sprouting. By inhibiting BDNF increases, LEV may be involved in sprouting inhibition, which at least partly, contributes to hippocampal neuronal reorganization. The neuroprotective effects of LEV have also been observed in kainic acid-induced toxicity in rat [30], and the stroke and head injury model in rat [11,43].

5. Conclusion

Prophylactic treatment with LEV inhibited hippocampal sclerosis-like changes characterized by neuronal loss, sprouting and increased BDNF observed in mature SERs. This inhibitory effect was, at least in part, attributable to LEV suppression of sprouting, an event probably due to up-regulation of BDNF expression and of neuronal death.

Conflict of interest

The authors declare no conflicts of interest.

Acknowledgement

This study was supported by UCB, Inc, Belgium. Levetiracetam was kindly provided by UCB, Inc, Belgium.

References

[1] T. Amano, H. Amano, H. Matsubayashi, K. Ishihara, T. Serikawa, M. Sasa, Enhanced Ca(2+) influx with mossy fiber stimulation in hippocampal CA3 neurons of spontaneously epileptic rats, Brain Res. 910 (2001) 199–203.
[2] J.A. Armijo, M. Shushtarian, E.M. Valdizan, A. Cuadrado, I. de las Cuevas, J. Adín, Ion channels and epilepsy, Curr. Pharm. Des. 11 (2005) 1975–2003.
[3] J.E. Cavazos, I. Das, T.P. Sutula, Neuronal loss induced in limbic pathways by kindling: evidence for induction of hippocampal sclerosis by repeated brief seizures, J. Neurosci. 14 (1994) 3106–3121.
[4] P. Czapinski, B. Blaszczyk, S.J. Czuczwar, Mechanisms of action of antiepileptic drugs, Curr. Top. Med. Chem. 5 (2005) 3–14.
[5] A.C. Errington, T. Stohr, G. Lees, Voltage gated ion channels: target for anticonvulsant drugs, Curr. Top. Med. Chem. 5 (2005) 15–30.
[6] P. Genton, B. Van Vleymen, Piracetam and levetiracetam: close structural similarities but different pharmacological and clinical profiles, Epileptic Disord. 2 (2000) 99–105.
[7] A.J. Gower, E. Hirsch, A. Boehrer, M. Noyer, C. Marescaux, Effects of levetiracetam, a novel antiepileptic drug, on convulsant activity in two genetic rat models of epilepsy, Epilepsy Res. 22 (1995) 207–213.
[8] R. Hanaya, M. Sasa, H. Ujihara, K. Ishihara, T. Serikawa, K. Iida, T. Akimitsu, K. Arita, K. Kurisu, Suppression by topiramate of epileptiform burst discharges in hippocampal CA3 neurons of spontaneously epileptic rat in vitro, Brain Res. 789 (1998) 274–282.
[9] R. Hanaya, Y. Kiura, K. Kurisu, N. Sakai, T. Serikawa, M. Sasa, N-acetyl-L-aspartate activates hippocampal CA3 neurons in rodent slice preparations, Brain Res. Bull. 75 (2008) 663–667.
[10] R. Hanaya, M. Sasa, S. Sugata, M. Tokudome, T. Serikawa, K. Kurisu, K. Arita, Hippocampal cell loss and propagation of abnormal discharges accompanied with the expression of tonic convulsion in the spontaneously epileptic rat, Brain Res. 1328 (2010) 171–180.

[11] E. Hanon, H. Klitgaard, Neuroprotective properties of the novel antiepileptic drug levetiracetam in the rat middle cerebral artery occlusion model of focal cerebral ischemia, Seizure 10 (2001) 287–293.
[12] K. Ishihara, M. Sasa, T. Momiyama, H. Ujihara, J. Nakamura, T. Serikawa, J. Yamada, S. Takaori, Abnormal excitability of hippocampal CA3 pyramidal neurons of spontaneously epileptic rats (SER), a double mutant, Exp. Neurol. 119 (1993) 287–290.
[13] Y. Ishimaru, S. Chiba, T. Serikawa, M. Sasa, H. Inaba, Y. Tamura, T. Ishimoto, H. Takasaki, K. Sakamoto, K. Yamaguchi, Effects of levetiracetam on hippocampal kindling in Noda epileptic rats, Brain Res. 1309 (2010) 104–109.
[14] C. Ji-qun, K. Ishihara, T. Nagayama, T. Serikawa, M. Sasa, Long-lasting antiepileptic effects of levetiracetam against epileptic seizures in the spontaneously epileptic rat (SER): differentiation of levetiracetam from conventional antiepileptic drugs, Epilepsia 46 (2005) 1362–1370.
[15] S.I. Johannessen, D. Battino, D.J. Berry, M. Bialer, G. Kramer, T. Tomson, P.N. Patsalos, Therapeutic drug monitoring of the newer antiepileptic drugs, Ther. Drug Monit. 25 (2003) 347–363.
[16] R.M. Kaminski, M. Gillard, K. Leclercq, E. Hanon, G. Lorent, D. Dassesse, A. Matagne, H. Klitgaard, Proepileptic phenotype of SV2A-deficient mice is associated with reduced anticonvulsant efficacy of levetiracetam, Epilepsia 50 (2009) 1729–1740.
[17] D.G. Kasteleijn-Nolst Trenité, E. Hirsc, Levetiracetam: preliminary efficacy in generalized seizures, Epileptic Disord. Suppl. 1 (2003) 39–44.
[18] K. Kitada, T. Akimitsu, Y. Shigematsu, A. Kondo, T. Maihara, N. Yokoi, T. Kuramoto, M. Sasa, T. Serikawa, Accumulation of N-acetyl-L-aspartate in the brain of the tremor rat, a mutant exhibiting absence-like seizure and spongiform degeneration in the central nervous system, J. Neurochem. 74 (2000) 2512–2519.
[19] H. Klitgaard, A. Matagne, J. Gobert, E. Wülfert, Evidence for a unique profile of levetiracetam in rodent models of seizures and epilepsy, Eur. J. Pharmacol. 353 (1998) 191–206.
[20] H. Klitgaard, Levetiracetam: the preclinical profile of a new class of antiepileptic drugs? Epilepsia 42 (Suppl. 4) (2001) 13–18.
[21] M. Knipper, L.S. Leung, D. Zhao, R.J. Rylett, Short-term modulation of glutamatergic in adult rat hippocampus by NGF, Neuroreport 5 (1994) 2433–2436.
[22] R. Koyama, M.K. Yamada, S. Fujisawa, R. Katoh-Semba, N. Matsuki, Y. Ikegaya, Brain-derived neurotrophic factor induces hyperexcitable reentrant circuits in the dentate gyrus, J. Neurosci. 24 (2004) 7215–7224.
[23] T. Kuramoto, K. Kitada, T. Inui, Y. Sasaki, K. Ito, T. Hase, S. Kawagachi, Y. Ogawa, K. Nakao, G.S. Barsh, M. Nagao, T. Ushijima, T. Serikawa, Attractin/mahogany/zitter plays a critical role in myelination of the central nervous system, Proc. Natl. Acad. Sci. U. S. A. 98 (2001) 559–564.
[24] I. Leppik, M. Morrell, P. Godfroid, C. Arrigo, Seizure-free days observed in randomized placebo-controlled add-on trials with levetiracetam in partial epilepsy, Epilepsia 44 (2003) 1232–1350.
[25] W. Löscher, Animal models of epilepsy for the development of antiepileptogenic and disease-modifying drugs. A comparison of the pharmacology of kindling and post-status epilepticus models of temporal lobe epilepsy, Epilepsy Res. 50 (2002) 105–123.
[26] W. Löscher, D. Hönack, Profile of ucb L059, a novel anticonvulsant drug, in models of partial and generalized epilepsy in mice and rats, Eur. J. Pharmacol. 232 (1993) 147–158.
[27] E.A. Lukyanetz, V.M. Shkryl, P.G. Kostyuk, Selective blockade of N-type calcium channels by levetiracetam, Epilepsia 43 (2002) 9–18.
[28] B.A. Lynch, N. Lambeng, K. Nocka, P. Kensel-Hammes, S.M. Bajjalieh, A. Matagne, B. Fuks, The synaptic vesicle protein SV2A is the binding site for the antiepileptic drug levetiracetam, Proc. Natl. Acad. Sci. U. S. A. 101 (2004) 9861–9866.
[29] D.G. Margineanu, H. Klitgaard, Levetiracetam has no significant gamma-aminobutyric acid-related effect on paired-pulse interaction in the dentate gyrus of rats, Eur. J. Pharmacol. 466 (2003) 255–261.
[30] H. Marini, C. Costa, M. Passaniti, M. Esposito, G.M. Campo, R. Ientile, E.B. Adamo, R. Marini, P. Calabresi, D. Altavilla, L. Minutoli, F. Pisani, F. Squadrito, Levetiracetam protects against kainic acid-induced toxicity, Life Sci. 74 (2004) 1253–1264.
[31] T.R. Mhyre, C.D. Applegate, Persistent regional increases in brain-derived neurotrophic factor in the flurothyl model of epileptogenesis are dependent upon the kindling status of the animal, Neuroscience 121 (2003) 1031–1045.
[32] Y. Ohno, S. Ishihara, R. Terada, T. Serikawa, M. Sasa, Antiepileptogenic and anticonvulsive actions of levetiracetam in a pentylenetetrazole kindling model, Epilepsy Res. 89 (2010) 360–364.
[33] G. Paxinos, C. Watson, The Rat Brain in Stereotaxic Coordinates, 3rd ed., Academic Press, San Diego, 1996.
[34] A. Pitman, T.P. Sutula, Is epilepsy a progressive disorder? Process for new therapeutic approaches in temporal lobe epilepsy, Lancet Neurol. 1 (2002) 173–181.
[35] A. Represa, G. Le Gall La Salle, Y. Ben-Ari, Hippocampal plasticity in the kindling model of epilepsy in rats, Neurosci. Lett. 99 (1989) 345–350.
[36] S. Rhem, P. Mehraein, A.P. Anzil, F. Deerberg, A new rat mutant with detective overhairs and spongy degeneration of the central nervus system: clinical pathological studies, Lab. Animal Sci. 32 (1982) 70–73.
[37] M. Sasa, Y. Ohno, H. Ujihara, Y. Fujita, M. Yoshimura, S. Takaori, T. Serikawa, J. Yamada, Effects of antiepileptic drugs on absence-like and tonic seizures in the spontaneously epileptic rat, a double mutant rat, Epilepsia 29 (1988) 505–513.
[38] M. Sasa, A frontier in epilepsy: novel antiepileptogenetic drugs, J. Pharmacol. Sci. 100 (2006) 487–494.
[39] T. Serikawa, J. Yamada, Epileptic seizures in rats homozygous for two mutations, zitter and tremor, J. Hered. 77 (1986) 441–444.
[40] T. Serikawa, J. Yamada, H. Ujihara, Y. Ohno, M. Sasa, S. Takaori, Ontogeny of absence-like and tonic seizures in the spontaneously epileptic rat, Lab. Anim. 25 (1991) 216–221.
[41] S. Tokuda, N. Sofue, Y. Ohno, M. Sasa, T. Serikawa, Inhibitory effects of levetiracetam on absence seizures in a novel absence-like epilepsy animal model, Groggy rat, Brain Res. 1359 (2010) 298–303.
[42] L.V. Vinogradova, C.M. van Rijn, Anticonvulsive and antiepileptogenic effects of levetiracetam in the audiogenic kindling model, Epilepsia 49 (2008) 1160–1168.
[43] H. Wang, J. Gao, T.F. Lassiter, D.L. McDonagh, H. Sheng, D.S. Warner, J.R. Lynch, D.T. Laskowitz, Levetiracetam is neuroprotective in murine models of closed head injury and subarachnoid hemorrhage, Neurocrit. Care 5 (2006) 71–78.
[44] J. Yamada, T. Serikawa, J. Ishiko, T. Inui, H. Takada, Y. Kawai, A. Okaniwa, Rats with congenital tremor and curled whisker and hair, Exp. Anim. 34 (1985) 183–188.
[45] H.D. Yan, C. Ji-qun, K. Ishihara, T. Nagayama, T. Serikawa, M. Sasa, Separation of antiepileptogenic and antiseizure effects of levetiracetam in the spontaneously epileptic rat (SER), Epilepsia 46 (2005) 1170–1177.
[46] H.D. Yan, K. Ishihara, R. Hanaya, K. Kurisu, T. Serikawa, M. Sasa, Voltage-dependent calcium channel abnormalities in hippocampal CA3 neurons of spontaneously epileptic rats, Epilepsia 48 (2007) 758–764.
[47] D.M. Yilmazer-Hanke, H.K. Wolf, J. Scgeamm, C.E. Elger, O.D. Wiestler, I. Blumcke, Subregional pathology of the amygdale complex and entorhinal region in surgical specimen from patients with pharmacoresistant temporal lobe epilepsy, J. Neuropathol. Exp. Neurol. 59 (2000) 907–920.
[48] C. Zona, I. Niespodziany, C. Marchetti, H. Klitgaard, G. Bernardi, D.G. Margineanu, Levetiracetam does not modulate neuronal voltage-gated Na^+ and T-type Ca^{2+} currents, Seizure 10 (2001) 279–286.

BRAIN RESEARCH 1389 (2011) 161–168

available at www.sciencedirect.com

ScienceDirect

www.elsevier.com/locate/brainres

BRAIN RESEARCH

Research Report

Oligodendroglial pathology in the development of myelin breakdown in the *dmy* mutant rat

Mitsuru Kuwamura[a,*], *Kazuo Inumaki*[a], *Miyuu Tanaka*[a], *Makoto Shirai*[a], *Takeshi Izawa*[a], *Jyoji Yamate*[a], *Robin J.M. Franklin*[b], *Takashi Kuramoto*[c], *Tadao Serikawa*[c]

[a]*Laboratory of Veterinary Pathology, Osaka Prefecture University, Izumisano, Osaka 598–8531, Japan*
[b]*MRC Cambridge Centre for Stem Cell Biology and Regenerative Medicine and Department of Veterinary Medicine, University of Cambridge, Madingley Road, Cambridge CB3 0ES, UK*
[c]*Institute of Laboratory Animals, Graduate School of Medicine, Kyoto University, Sakyo-ku, Kyoto 606–8501, Japan*

ARTICLE INFO

Article history:
Accepted 3 March 2011
Available online 9 March 2011

Keywords:
Dysmyelination
Mutant rat
Oligodendrocyte
Oligodendrocyte progenitor cell
Mitochondria

ABSTRACT

The *dmy* rat is an autosomal recessive mutant that exhibits severe myelin destruction throughout the white matter of the central nervous system. Recently, a point mutation in intron 3 of the Mrs2 has been found in the *dmy* rat. Mrs2 encodes an essential component of the major electrophoretic Mg^{2+} influx system in mitochondria of yeast as well as human cells. In this study, we examined the morphological and numerical changes of oligodendroctyes in the development of myelin destruction in the spinal cord of the *dmy* rat. The number of oligodendrocytes decreases rapidly from 7 weeks of age in the *dmy* rat in accordance with myelin breakdown. Hypertrophic oligodendrocytes were frequently observed, and the cytoplasm was found to be intensely positive for prohibitin and cytochrome oxidase, mitochondrial markers. These data suggest that mitochondrial dysfunction causes a work/compensatory hypertrophy of oligodendrocytes, resulting in direct cell death and leading to myelin destruction.

1. Introduction

Myelin mutant animals, in which myelination is disrupted by a genetic perturbation, have helped with the identification of genes associated with myelination and are useful in increasing our understanding of the function of specific genes in the proper spatial and temporal context of development and disease (Griffiths, 1996). Mutations of structural myelin components have been investigated in many mice and rat models (Al-Saktawi et al., 2003; Griffiths, 1996; Knapp et al., 1986, 2009; Kwiecien et al., 1998). Despite a direct deficit in myelin components, the process of myelination and maintenance of myelin involves complex mechanisms such as the production and transport of myelin-related proteins and lipids. For example, abnormalities of microtubules are considered to be responsible for the hypomyelination and progressive demyelination of the CNS in the *taiep* rat (Duncan et al., 1992; Song et al., 1999). The developmental regulation

* *Corresponding author.* Fax: +81 72 463 5346.
E-mail address: kuwamura@vet.osakafu-u.ac.jp (M. Kuwamura).
Abbreviations: CNS, central nervous system; OPCs, oligodendrocyte progenitor cells; PLP, proteolipid protein

0006-8993/$ – see front matter © 2011 Elsevier B.V. All rights reserved.
doi:10.1016/j.brainres.2011.03.009

and maintenance of myelin have been widely investigated, but many details of these processes remain to be clarified.

The *dmy* rat is an autosomal recessive mutant that exhibits hind limb ataxia and severe myelin destruction throughout the white matter of the central nervous system (CNS) during the late stage of myelination (Kuramoto et al., 1996; Kuwamura et al., 2004). The causative gene of the *dmy* rat is located on rat chromosome 17, homologous to human chromosome 6 and mouse chromosome 13 (Kuramoto et al., 1996). There are no myelin-related or myelin disorder-related genes in the homologous regions of humans and mice, suggesting that the *dmy* rat is a novel myelin mutant and that the causative gene may play a crucial role in the adequate maintenance of myelin. Recently, Kuramoto et al. have revealed that the *dmy* rat has a point mutation generating a novel splicing acceptor site in intron 3 of the Mrs2 gene (Kuramoto et al., 2011). Mrs2 encodes an essential component of the major electrophoretic Mg2+ influx system in mitochondria of yeast as well as human cells, suggesting that the *dmy* mutation is associated with mitochondrial dysfunction.

In this study, we examined the morphological and numerical changes of oligodendroctyes in the development of myelin destruction in the spinal cord of the *dmy* rat. Our results indicate that the number of oligodendrocytes decreases rapidly from 7 weeks of age in the *dmy* rat in accordance with myelin breakdown. Hypertrophic oligodendrocytes were frequently observed, and the cytoplasm was found to be intensely positive for prohibitin and cytochrome oxidase, mitochondrial markers. These data suggest that mitochondrial dysfunction causes a work/compensatory hypertrophy of oligodendrocytes, resulting in direct cell death and leading to myelin destruction.

2. Results

2.1. *Number of oligodendrocytes*

No remarkable histopathological myelin-related lesions were found in the *dmy* rat up to 6 weeks of age. In the *dmy* rat at 7–10 weeks, pale staining areas developed in the white matter of the CNS, with the ventral funiculus being affected particularly severely compared with the dorsal funiculus in the spinal cord (Fig. 1). We investigated the number of oligodendrocytes during the development of myelin destruction in the *dmy* rat by using the proteolipid protein (PLP) in situ hybridization. Until 6 weeks of age, there was no significant difference in the cell number and morphology of PLP-expressing cells between control and *dmy* rats (Fig. 2a–h and Fig. 3a, b). At 7 weeks, the cell density of the oligodendrocytes was significantly decreased and the myelin was rapidly collapsing at 8 weeks in the ventral funiculus (Figs. 2i–p and 3b). The cell density in the dorsal funiculus was retained at all of the weeks examined.

2.2. *Number of OPCs*

The numerical changes of OPCs were examined by NG2 immunohistochemistry (Bu et al., 2004; Kitada and Rowitch, 2006). No morphological abnormalities were found in the NG2-positive cells between control and *dmy* rats until 4 weeks. At 4 weeks, no difference in the cell density of NG2 was observed between control and *dmy* rats in either the dorsal or ventral funiculi. At 6 and 7 weeks, the density of NG2 in the ventral funiculus of *dmy* rat was increased (Fig. 3c, d and Fig. 4a, b); afterwards, at 8 weeks, the density rapidly began to decrease

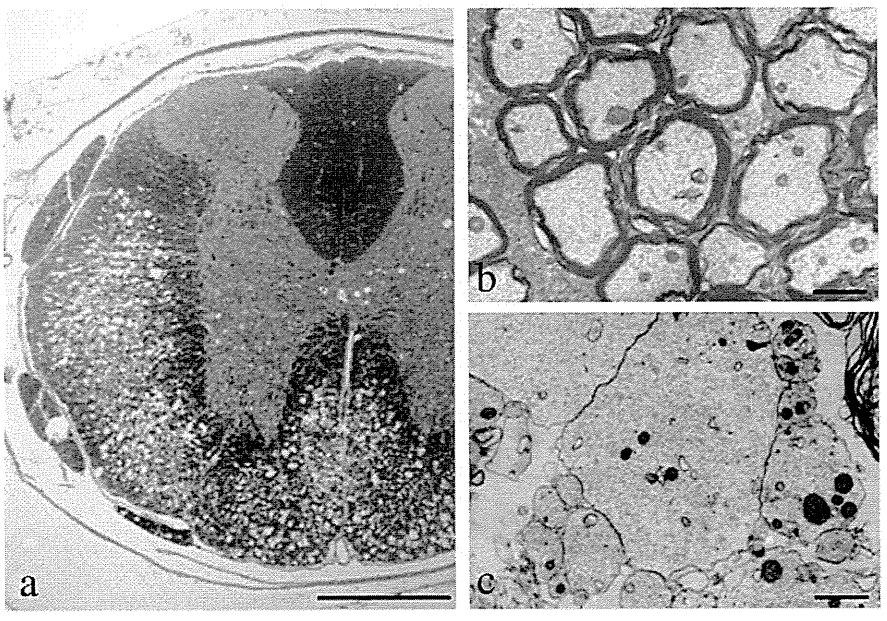

Fig. 1 – Epon embedded toluidine blue stained section of the thoracic spinal cord of 7-week-old *dmy/dmy* rat (a). Marked destruction of myelin is distributed in the lateral and ventral parts, whereas the dorsal funiculus remained normal appearance. Bar, 500 μm. Electron microscopy of the thoracic spinal cord of 7-week-old *dmy/dmy* rat. Normal myelinated axons are found in the dorsal funiculus (b). Many naked axons are seen in the ventral funiculus (c). Bar, 1 μm.